Analysis and Simulation for Laser-Compton Cooling of Electron Beams

T. Ohgaki
Lawrence Berkeley National Laboratory, Berkeley, California 94720
(October 1999)

The method of the Laser-Compton cooling of the electron beams is studied. Using a Monte Carlo code, we have evaluated the effects of the Laser-electron interaction for cooling. The optics with and without chromatic correction for cooling are examined. Problems of the optics for cooling are discussed.

I. INTRODUCTION

The new method of the electron beam cooling for future linear colliders is proposed by V.Telnov [1]. During a collision with laser photons, the transverse distribution of electrons remains almost unchanged and also the angular spread is almost constant. Because the Compton scattered photons follow the initial electron trajectory with a small additional spread due to much lower energy of photons (a few eV) than the energy of electrons (several GeV). The emittance $\epsilon_i = \sigma_i \sigma_i'$ remains almost unchanged. At the same time, the electron energy decreases from E_0 to E_f. Thus the normalized emittances have decreased as follows

$$\epsilon_n = \gamma\epsilon = \epsilon_{n0}(E_f/E_0), \tag{1}$$

where ϵ_{n0} and ϵ_n are the initial and final normalized emittances.

In this paper, we have evaluated the effects of the Laser-Compton interaction for cooling using a Monte Carlo code [2]. This simulation calculates the effects of the nonlinear Compton scattering between the laser photons and the electrons during the multi-cooling stage, but it does not include the optics and the reacceleration linac for cooling. Next, we consider the optics for cooling with and without chromatic correction. A summary of the conclusion is given in section IV.

II. LASER-ELECTRON INTERACTION

A. Laser-Electron Interaction

In this section, we describe the main parameters for Laser-Compton cooling of electron beams. A laser photon of energy ω_L (wavelength λ_L) is scattered by an electron beam of energy E_e in the interaction point (IP). The kinematics of Compton scattering is characterized by the dimensionless parameter [1]

$$x \equiv \frac{4E_e\omega_L}{m_e^2c^4} \approx 0.019 \left[\frac{E_e}{\mathrm{GeV}}\right]\left[\frac{\mu\mathrm{m}}{\lambda_L}\right], \tag{2}$$

where m_e is electron mass. The parameters of the electron and laser beams for Laser-Compton cooling are listed in Table I and II, and then x=0.2.

The ratio of normalized emittances before and after the collision of the Laser-electron beams is

$$\begin{aligned} C = \frac{E_0}{E_f} &= 1 + \frac{1}{E_f}\int \frac{dE}{dz}dz \\ &= 1 + \frac{1}{E_f}\int \frac{2}{3}r_e^2\gamma^2 B^2 dz \\ &= 1 + \frac{16\sqrt{2}\pi^{3/2}r_e^2\gamma_0}{3m_ec^2 l_L\lambda_L}\exp\left(\frac{8Z_R^2}{l_L^2}\right)\left(1-\mathrm{erf}\left(\frac{2\sqrt{2}Z_R}{l_L}\right)\right)A, \end{aligned} \tag{3}$$

where E_0 and E_f are the initial and final energies of electron beams, $\gamma_0 = E_0/m_ec^2$, $l_L(\sim 2\sigma_L)$ the length of the laser pulse, Z_R the Rayleigh length, A the laser pulse energy. In our case, the ratio C is 5 from the simulation result.

The required laser flush energy is

$$A[J] = \frac{3\sqrt{2}m_e c^2 l_L \lambda_L}{32\pi^{3/2} r_e^2 \gamma_0} \exp\left(-\frac{8Z_R^2}{l_L^2}\right)\left(1 - \mathrm{erf}\left(\frac{2\sqrt{2}Z_R}{l_L}\right)\right)^{-1}(C-1), \tag{4}$$

or the simplified formula is [1]

$$A[J] = 100\frac{\lambda_L[\mu\mathrm{m}]\, l_e[\mathrm{mm}]}{E_0[\mathrm{GeV}]}(C-1), \tag{5}$$

where $l_e(\sim 2\sigma_z)$ is the bunch length of electron beams. In our case, A is 20 J and the nonlinear parameter $\xi = 1.5$.

The ratio of energy spread is defined as

$$\delta = \sigma_e / E_e, \tag{6}$$

where σ_e is the rms energy of the electron beams.

The equilibrium emittance due to the Compton scattering is [1]

$$\epsilon_{ni,\min} = \frac{7.2 \times 10^{-10}\beta_i[\mathrm{mm}]}{\lambda_L[\mu\mathrm{m}]}\ \mathrm{m}\cdot\mathrm{rad}\ (i = x, y). \tag{7}$$

In the following section, we use these formulas and compare them with the simulation results.

B. Simulation of Laser-Electron Interaction

For simulation the electron beams are simply assumed to be round beams. The parameters of the electron beams are listed in Table I. The parameters of the laser beams are listed in Table II. The one stage for cooling consists two parts as follows:

1. The Laser-Compton interaction between the electron and laser beams.

2. The reacceleration of electrons in linac.

In the first part, we simulated the interactions by the CAIN code [2]. In order to accelerate the electron beams to 5 GeV in the second part, we simply added the energy $\Delta E = 5\ \mathrm{GeV} - E_{ave}$ for reacceleration, where E_{ave} is the average energy of the scattered electron beams after Laser-Compton interactions. The β_x and β_y at the IP are fixed to be 0.1 mm. The initial energy spread of the electron beams is 1%. The polarization of the electron and laser beams are P_e=1 and P_L=1 (circular polarization), respectively. When the x parameter is small, the spectrum of the scattered photons does not depend on the polarization combination.

Here we define the transverse, longitudinal, and 6D emittances in the simulation. The x-transverse emittance is

$$\epsilon_{n,x} = \sqrt{\sigma_x^2\sigma_{x'}^2 - (< x\cdot x' > - < x >< x' >)^2} \tag{8}$$

where the symbol <> means to take an average of all particles in a bunch.

The y-transverse emittance is

$$\epsilon_{n,y} = \sqrt{\sigma_y^2\sigma_{y'}^2 - (< y\cdot y' > - < y >< y' >)^2}. \tag{9}$$

The longitudinal emittance is

$$\epsilon_{n,l} = \sqrt{\sigma_l^2\sigma_{p_z}^2 - (< z\cdot p_z > - < z >< p_z >)^2}/(m_e c). \tag{10}$$

The 6D emittance is defined as

$$\epsilon_{6N} = \epsilon_{n,x}\cdot\epsilon_{n,y}\cdot\epsilon_{n,l}. \tag{11}$$

Figure 1 shows the longitudinal distribution of the electrons after the first Laser-Compton scattering. The average energy of the electron beams is 1.0 GeV and the energy spread δ is 0.19. The longitudinal distribution seems likely a boomerang. If we assume the short Rayleigh length of the laser pulse, the energy loss of head and tail of the beams is small.

The transverse sizes of the electron beams in the multi-stage cooling are shown in Fig. 2. During a collision with laser photons, the transverse distribution of electrons remains almost unchanged. But they degrease when we focus them for next Laser-Compton interactions due to lower normalized emittance and fixed β-function ($\sigma_i = \sqrt{\beta_i \epsilon_{n,i}/\gamma}$). The angles of the electron beams in the multi-stage cooling are shown in Fig. 3. As a result of reacceleration, the angles of the electrons decrease. They increase when we focus them for next Laser-Compton interactions. Finally the angles attain the average of Compton scattering angle and the effect of cooling saturates.

Figure 4 shows the transverse emittances of the electron beams in the multi-stage cooling. They degrease when the electron beams reaccelerate. From Eq.(7), $\epsilon_{ni,\min} = 1.4 \times 10^{-10}$ m·rad, and the simulation presents $\epsilon_{ni,\min} = 1.2 \times 10^{-9}$ m·rad. Figure 5 shows the longitudinal emittance of the electron beams in the multi-stage cooling. Due to the increase from the energy spread 1% of the initial beams to 20% after Compton scattering, the longitudinal emittance rapidly increases at the first stage. After the first stage, the normalized longitudinal emittance are stable. The 6D emittance of the electron beams in the multi-stage cooling is shown in Fig. 6. The second cooling stage has the most largest gain for cooling. The 8th or 9th cooling stages have small gain for cooling. The initial and final 6D emittances ϵ_{6N} are 1.5×10^{-13} and 1.2×10^{-19} (m·rad)^3, respectively.

Figure 7 shows the polarization of the electron beams in the multi-stage cooling. The final polarization P_e after multi-stage cooling is 0.54.

III. OPTICS DESIGN FOR LASER-COMPTON COOLING

A. Linear Optics

There are three optical devices for Laser-Compton cooling of electron beams as follows:

1. The focus optics to the first IP.
2. The defocus optics from the first IP to the reacceleration linac.
3. The focus optics from the linac to the next IP.

Figure 8 shows a schematics of the Laser-Compton cooling of electron beams. The optics 1 is focusing the electron beams from a few meters of β-function to several millimeters in order to effectively interact them with the laser beams. The optics 2 is defocusing them from several millimeters to a few meters for reacceleration of the electron beams in linac. In a multi-stage cooling system, the optics 3 is needed for cooling in the next stage. The problem for the focus and defocus optical devices is the energy spread of electrons and the electron beams with a large energy spread are necessary to correct the chromatic aberrations avoiding emittance growth.

In this subsection, we discuss the linear optics for Laser-Compton cooling without chromatic corrections. For the focus and defocus of the beams, we use the final doublet system which is similar to that of the final focus system of the future linear colliders [5]. The pole-tip field of the final quadrupole B_T is limited to 1.2 T and the pole-tip radius a is greater than 3 mm. The strength of the final quadrupole is

$$\kappa = B_T/(aB\rho) \leq 120/E(\mathrm{GeV}), \tag{12}$$

where B, ρ, and E are the magnetic field, the radius of curvature and the energy of the electron beams. In our case, the electron energies in the optics 1, 2, and 3 are 5.0, 1.0, and 5.0 GeV, respectively and the limit of the strength of the quadrupole in Laser cooling is larger than that of the final quadrupole of the future linear colliders. Due to the low energy beams in Laser cooling, the synchrotron radiation from quadrupoles and bends is negligible.

The difference of the three optical devices is the amount of the energy spread of the beams. In the optics 1,2, and 3, the beams have one, several tens, and a few % energy spread. In order to minimize the chromatic aberrations, we need to shorten the length between the final quadrupole and the IP. In this study the length from the face of the final quadrupole to the IP l is assumed to be 2 cm. Here we estimated the emittance growth in the optics 2, because the chromatic effects in the optics 2 is the most serious. Figure 9 shows the defocus linear optics for the Laser-Compton cooling by the MAD code [6]. The input file is attached to Appendix A. The energy of the electron beam is 1 GeV and the gain C is 5. The initial β_x and β_y after Laser-Compton interaction are 20 and 4 mm, respectively. The final β_x and β_y are assumed to be 2 and 1 m, respectively. The initial and final $\alpha_{x(y)}$ with no energy spread $\delta = 0$ are 0 in this optics. The strength κ of the final quadrupole for the beam energy of 1 GeV from Eq. (12) is assumed to be 120 m^{-2}.

The chromatic functions in the MAD are defined as

$$\xi_i = \sqrt{a_i^2 + b_i^2} \qquad (i = x, y), \tag{13}$$

$$b_i = \frac{1}{\beta_i}\frac{d\beta_i}{d\delta_s}, \tag{14}$$

$$a_i = \frac{d\alpha_i}{d\delta_s} - \frac{\alpha_i}{\beta_i}\frac{d\beta_i}{d\delta_s}. \tag{15}$$

where $\delta_s = \Delta p_s/p_0$ is the the difference of the reference momentum and the design momentum, divided by the reference momentum. In our case, the chromatic functions ξ_x and ξ_y are 18 and 148, respectively. The momentum dependence of the emittances in the defocus linear optics is shown in Fig. 10. In the paper [3], the analytical study by the thin-lens approximation has been studied for the focusing system, and here the transverse emittances are calculated by a particle-tracking simulation. The 10000 particles are tracked for the transverse and longitudinal Gaussian distribution by the MAD code. The relative energy spread δ is changed from 0 to 0.4. Due to the larger chromaticity ξ_y, the emittance ϵ_y is rapidly increasing with the energy spread δ. If we set a limit of 200% for $\Delta\epsilon_i/\epsilon_i$ $(i = x, y)$, the permissible energy spread δ_x and δ_y are 0.11 and 0.012 which mean the momentum band width $\pm 22\%$ and $\pm 2.4\%$, respectively. The results are not sufficient for cooling with $C = 5$, because the beams through the defocusing optics have several tens % of the energy spread. On the one hand, the optics can be useful as the optics 1 and 3 with a few % of the energy spread.

B. Non-Linear Optics

The linear optics for the optics 2 does not work as we seen before subsection. In this subsection we apply the chromaticity correction for the optics 2. The lattice for cooling is designed referring to the final focus system of future linear colliders by Oide [4]. The final doublet system is the same lattice as the linear optics. The method of chromaticity correction uses one family of sextupole to correct for vertical chromaticity and moreover we added two weak sextupoles in the lattice to correct for horizontal chromaticity. In order to cancel geometric aberrations the sextupoles are placed by the $-I$ transformation. Figure 11 shows the defocus nonlinear optics for the Laser-Compton cooling. The input file is attached to Appendix B. The total length of the lattice is about 63 m.

The momentum dependence of the emittances in the defocus nonlinear optics is shown in Fig. 12. The 10000 particles are tracked for the transverse and longitudinal Gaussian distribution by the MAD code. The relative energy spread δ is changed from 0 to 0.06 with the conservation $\kappa_2\ \theta_B$ where κ_2 and θ_B are the strength of the sextupole and the angle of the bending magnet. The initial β_x and β_y after Laser-Compton interaction are 20 and 4 mm, respectively. The final β_x and β_y are assumed to be 2 and 1 m, respectively. The initial and final $\alpha_x(y)$ with no energy spread $\delta = 0$ are 0 in this optics. After the chromaticity correction, the chromaticity functions ξ_x and ξ_y are 9.3 and 1.6, respectively. If we set a limit of 200% for $\Delta\epsilon_i/\epsilon_i (i = x, y)$, the permissible energy spread δ_x and δ_y are 0.040 and 0.023 which mean the momentum band width $\pm 8\%$ and $\pm 4.6\%$, respectively. By the comparison with the results of the linear optics at a limit of 200% for $\Delta\epsilon_i/\epsilon_i (i = x, y)$, the ϵ_y of the nonlinear optics is about two times larger than that of the linear one, but the ϵ_x of the nonlinear optics is three times smaller than that of the linear one. The results are still not sufficient for cooling with $C = 5$. These results emphasize the need to pursue further ideas for plasma lens [7].

In this paper, we have only estimated the focusing and defocusing optics for cooling. The other problem is the emittance growth of the beams in the reacceleration linac, because the emittance growth depends on the square of the energy spread of the beams.

IV. SUMMARY

We have presented the preliminary simulation results for Laser-Compton cooling of electron beams. The effects of the Laser-Compton interaction for cooling have been evaluated by the Monte Carlo simulation. From the simulation, we presented that the low emittance beams with $\epsilon_{6N} = 1.2 \times 10^{-19}$ (m·rad)^3 can be achieved in our beam parameters.

We made the optics with and without chromatic correction for cooling, but the optics are not sufficient for cooling due to the large energy spread of the electron beams.

For construction of the Laser-Compton cooling system, we need to solve the following problems:

1. Design of defocusing optics with a large energy spread from 10 to 20%.

2. Emittance growth of the beams with a large energy spread in the reacceleration linac.

V. APPENDIX

A. Defocusing Linear Optics

```
Title,"Defocusing Optics of Laser Cooling of Electrons for MAD version 8"
!
!define cell FFS
LX1: DRIFT, L= 0.0200000
LC2: DRIFT, L= 1.587360E-02
LC3: DRIFT, L= 2.534700E+00
QC1: QUADRUPOLE, L= 0.1200000, K1= 1.200000E+02
QC2: QUADRUPOLE, L= 0.1200000, K1= -1.130511E+02
QC3: QUADRUPOLE, L= 0.1200000, K1= 5.290453E+01
FFS: LINE=(LX1, QC1, QC2, LC2, QC3, LC3)
USE, FFS
PRINT, FULL
TWISS, SAVE, FFS, BETX=20.0E-3, BETY=4.0E-3, ALFX=0, ALFY=0,
DELTAP=0.0, CHROM, TAPE='twiss'
PLOT, TABLE=TWISS, HAXIS=S, VAXIS1=BETX,BETY, VAXIS2=DX,DY
PLOT, TABLE=TWISS, HAXIS=S, VAXIS1=WX,WY, VAXIS2=MUX,MUY
PLOT, TABLE=TWISS, HAXIS=S, VAXIS1=BETX, BETY, VAXIS2=MUX,MUY
BEAM, PARTICLE=ELECTRON, ENERGY=1.0,
EX=5.42E-10, EY=8.18E-12, ET=0.2*0.2E-3,
SIGE=0.2E0, SIGT=0.2E-3
TRACK
DO, TIMES=10000
START, X=3.29E-6*GAUSS(), Y=1.81E-7*GAUSS(),
PX=1.65E-4*GAUSS(), PY=4.52E-5*GAUSS(),
DELTAP=0.05E0*GAUSS(), T=0.2E-3*GAUSS()
ENDDO
RUN, TURNS=1, METHOD=TRANSPORT, FPRINT=1, TABLE=TWISS
ENDTRACK
STOP
```

B. Defocusing Non-Linear Optics

```
Title,"Defocusing Optics of Laser Cooling of Electrons for MAD version 8"
!
!define cell FFS
LX1: DRIFT, L= 0.0200000
LC2: DRIFT, L= 1.587360E-02
LC3: DRIFT, L= 2.534700E+00
QC1: QUADRUPOLE, L= 0.1200000, K1= 1.200000E+02
QC2: QUADRUPOLE, L= 0.1200000, K1= -1.130511E+02
QC3: QUADRUPOLE, L= 0.1200000, K1= 5.290453E+01
LN1: DRIFT, L= 5.591916E+00
LN2: DRIFT, L= 1.676474E+01
QN1: QUADRUPOLE, L= 0.4000000, K1= 1.120510E-01
QN2: QUADRUPOLE, L= 0.4000000, K1= -8.055034E-01
QN3: QUADRUPOLE, L= 0.4000000, K1= 4.135418E-01
QN4: QUADRUPOLE, L= 0.4000000, K1= -2.344771E-01
QN5: QUADRUPOLE, L= 0.4000000, K1= 2.719069E-01
SD1: SEXTUPOLE, L= 1.0000000, K2= -128
SD2: SEXTUPOLE, L= 1.0000000, K2= 15
B01: RBEND, L= 2.000000, ANGLE= 4.169559E-04
B02: RBEND, L= 2.000000, ANGLE= 1.317380E-04
```

```
M01: MARKER
FFS1: LINE=(LX1, QC1, QC2, LC2, QC3, LC3)
FFS2: LINE=(B01, QN1, QN2, LN1, SD2, QN3, LN2, QN4, M01,
SD1, B02, QN5, B02, SD1, QN4, LN2,
QN3, SD2, LN1, QN2, QN1, B01)
FFS: LINE=(FFS1, FFS2)
USE, FFS1
USE, FFS2, SYMM
USE, FFS
PRINT, FULL
TWISS, SAVE, FFS, BETX=20.0E-3, BETY=4.0E-3, ALFX=0, ALFY=0,
DELTAP=0.0, CHROM, TAPE='twiss'
PLOT, TABLE=TWISS, HAXIS=S, VAXIS1=BETX,BETY, VAXIS2=DX,DY
PLOT, TABLE=TWISS, HAXIS=S, VAXIS1=WX,WY, VAXIS2=MUX,MUY
PLOT, TABLE=TWISS, HAXIS=S, VAXIS1=BETX, BETY, VAXIS2=MUX,MUY
BEAM, PARTICLE=ELECTRON, ENERGY=1.0,
EX=5.42E-10, EY=8.18E-12, ET=0.2*0.2E-3,
SIGE=0.2E0, SIGT=0.2E-3
TRACK
DO, TIMES=10000
START, X=3.29E-6*GAUSS(), Y=1.81E-7*GAUSS(),
PX=1.65E-4*GAUSS(), PY=4.52E-5*GAUSS(),
DELTAP=0.0E0*GAUSS(), T=0.2E-3*GAUSS()
ENDDO
RUN, TURNS=1, METHOD=TRANSPORT, FPRINT=1, TABLE=TWISS
ENDTRACK
STOP
```

TABLE I. Parameters of electron beams for Laser-Compton cooling at $E_0 = 5$ GeV and $C = 5$.

E_0 (GeV)	N_{bunch}	$\epsilon_{n,x}/\epsilon_{n,y}$ (m·rad)	β_x/β_y (mm)	σ_x/σ_y (nm)	σ_z (mm)
5	10^{10}	$3.0 \times 10^{-6}/3.0 \times 10^{-6}$	0.1/0.1	170/170	0.2

TABLE II. Parameters of laser beams for Laser-Compton cooling at $E_0 = 5$ GeV and $C = 5$.

λ_L (μm)	A (J)	$R_{L,x}/R_{L,y}$ (mm)	$\sigma_{L,x}/\sigma_{L,y}$ (μm)	$\sigma_{L,z}$ (mm)
0.5	20	0.1/0.1	2.0/2.0	0.4

TABLE III. Parameters of electron beams for Laser-Compton cooling at $E_0 = 5$ GeV and $C = 5$ for the optics design.

E_0 (GeV)	$\epsilon_{n,x}/\epsilon_{n,y}$ (m·rad)	β_x/β_y (mm)	σ_x/σ_y (m)	σ_z (mm)
5	$1.06 \times 10^{-6}/1.6 \times 10^{-8}$	20/4	$3.3 \times 10^{-5}/1.8 \times 10^{-7}$	0.2

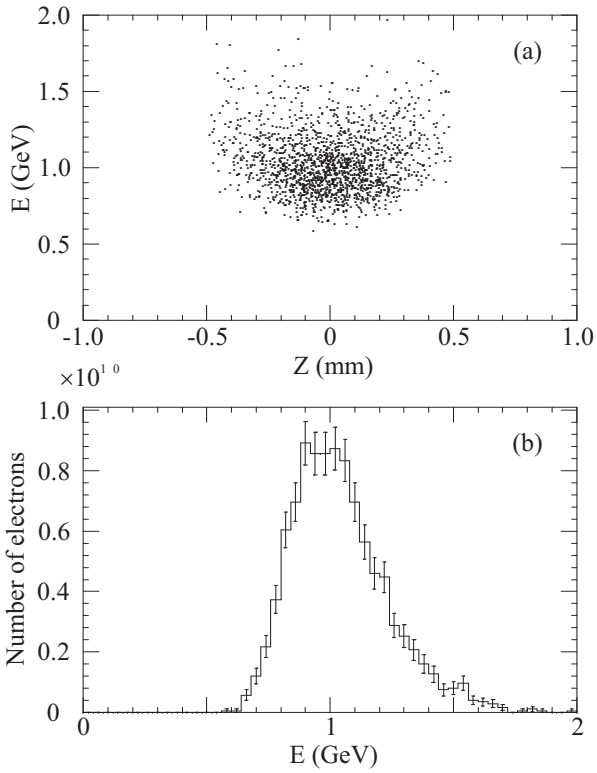

FIG. 1. The longitudinal distribution of the electrons. (a) The energy *vs.* z. (b) The energy distribution of the electrons.

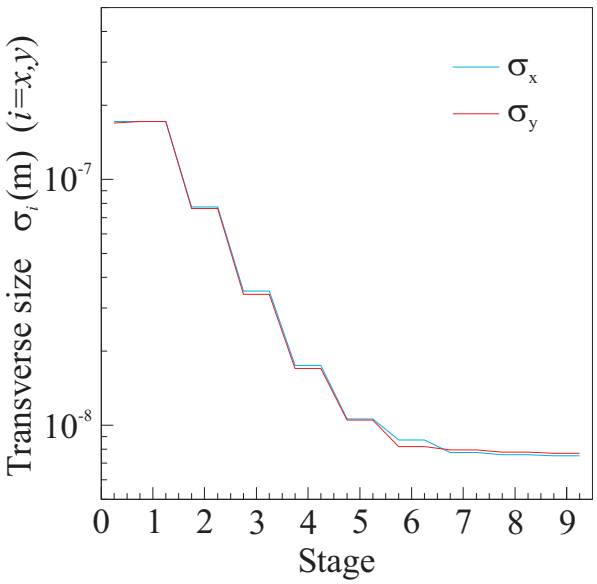

FIG. 2. The transverse sizes of the electron beams.

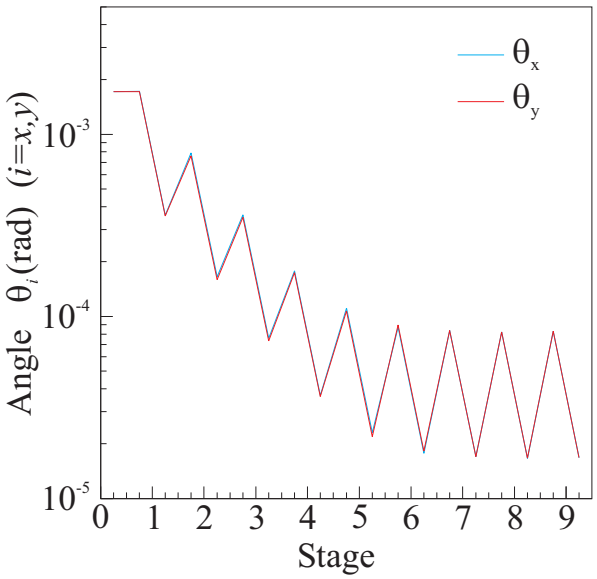

FIG. 3. The angles of the electron beams.

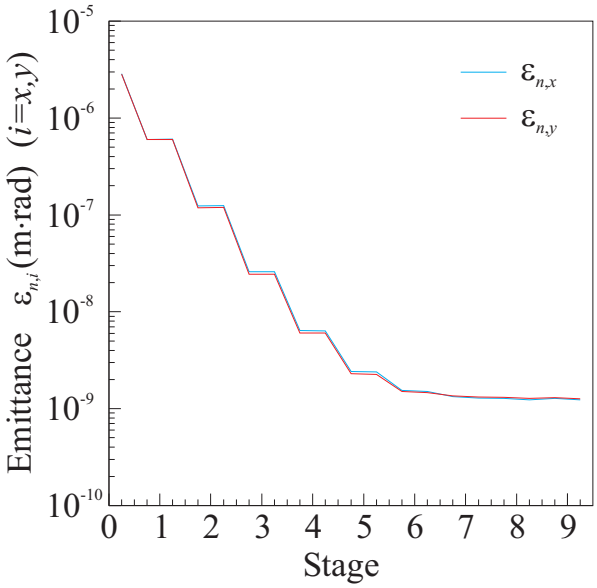

FIG. 4. The transverse emittances of the electron beams.

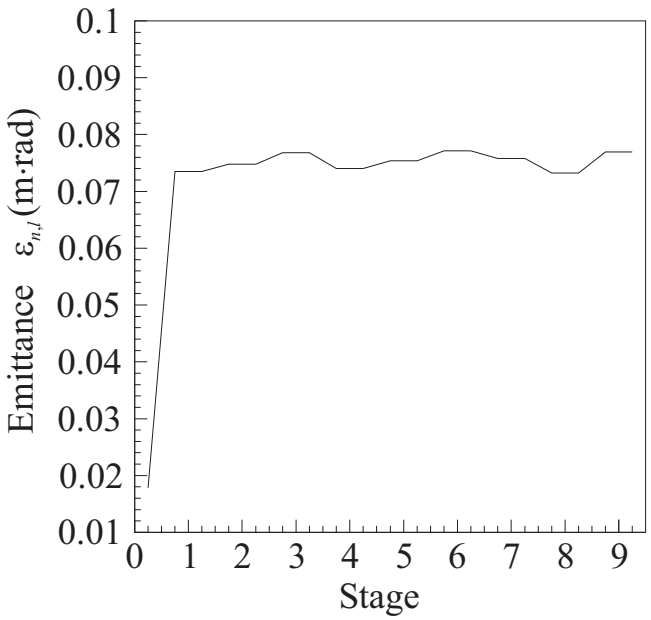

FIG. 5. The longitudinal emittance of the electron beams.

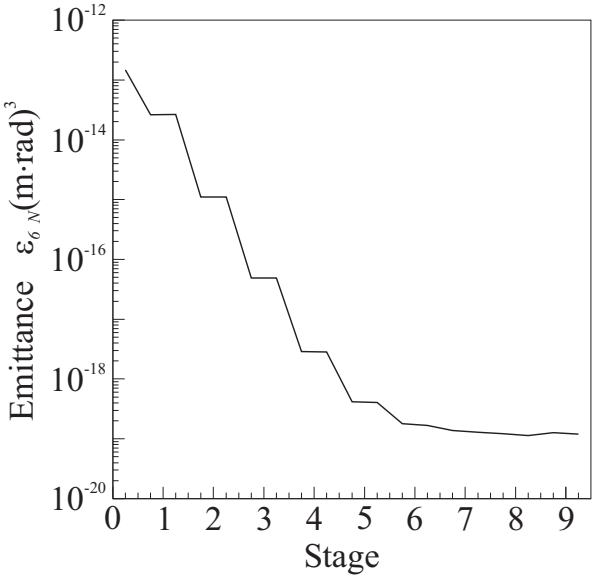

FIG. 6. The 6D emittance of the electron beams.

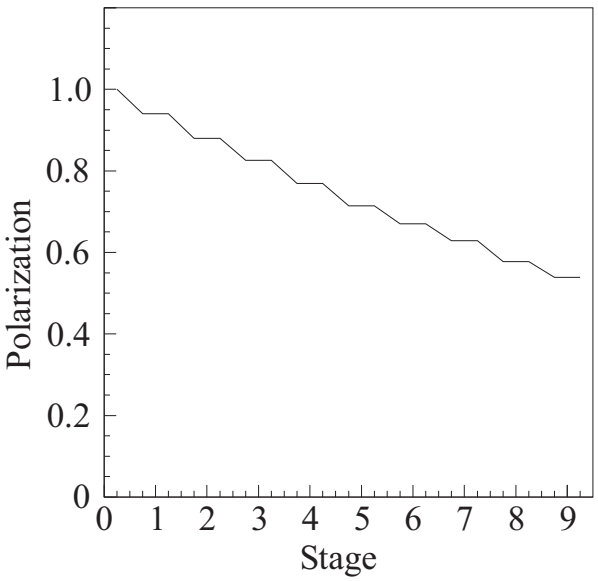

FIG. 7. The polarization of the electron beams.

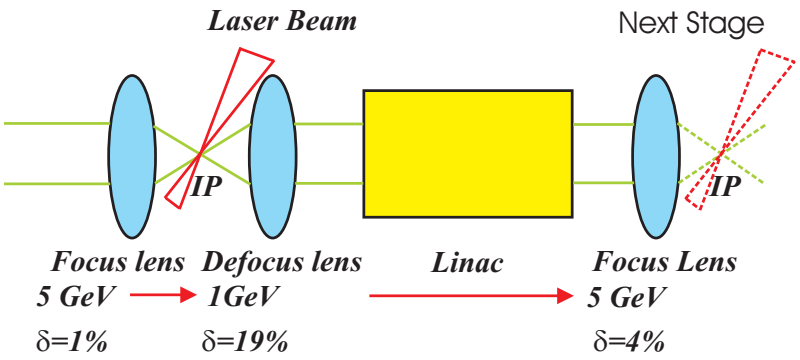

FIG. 8. Schematics of the Laser-Compton cooling of electron beams.

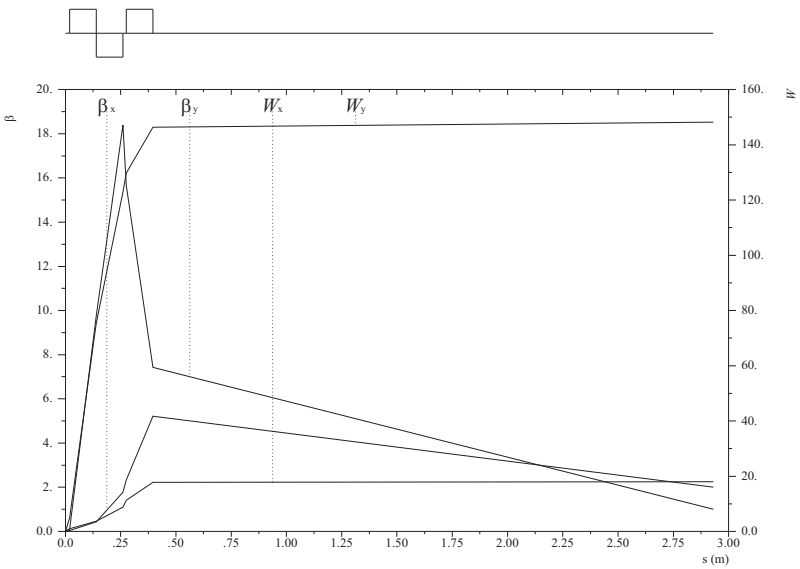

FIG. 9. The defocus linear optics for the Laser-Compton cooling.

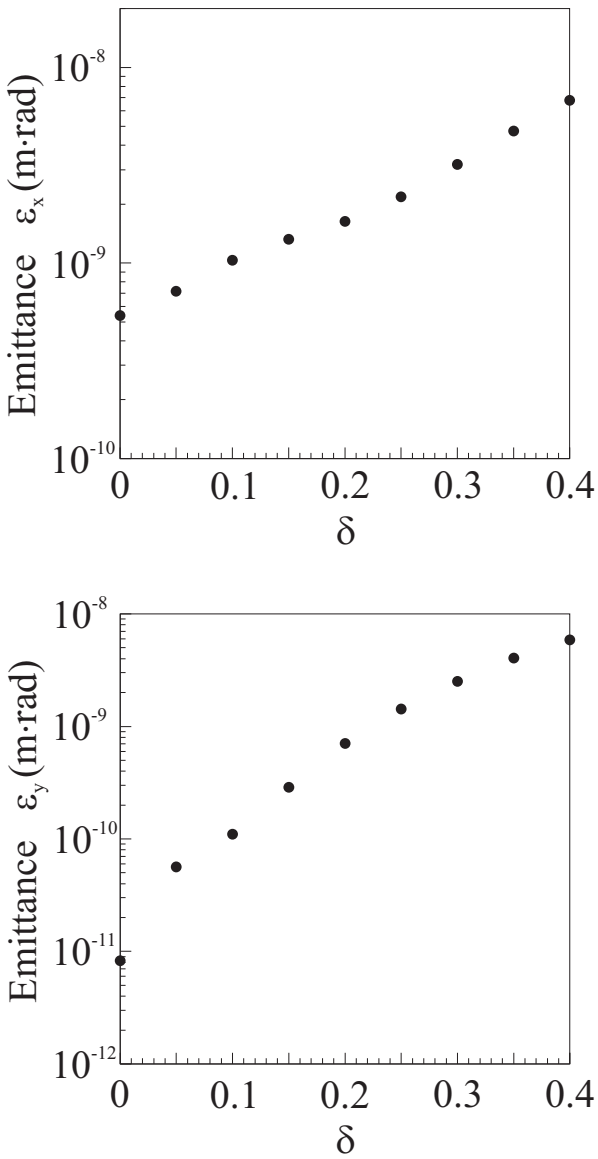

FIG. 10. Momentum dependence of the emittances in the defocus linear optics.

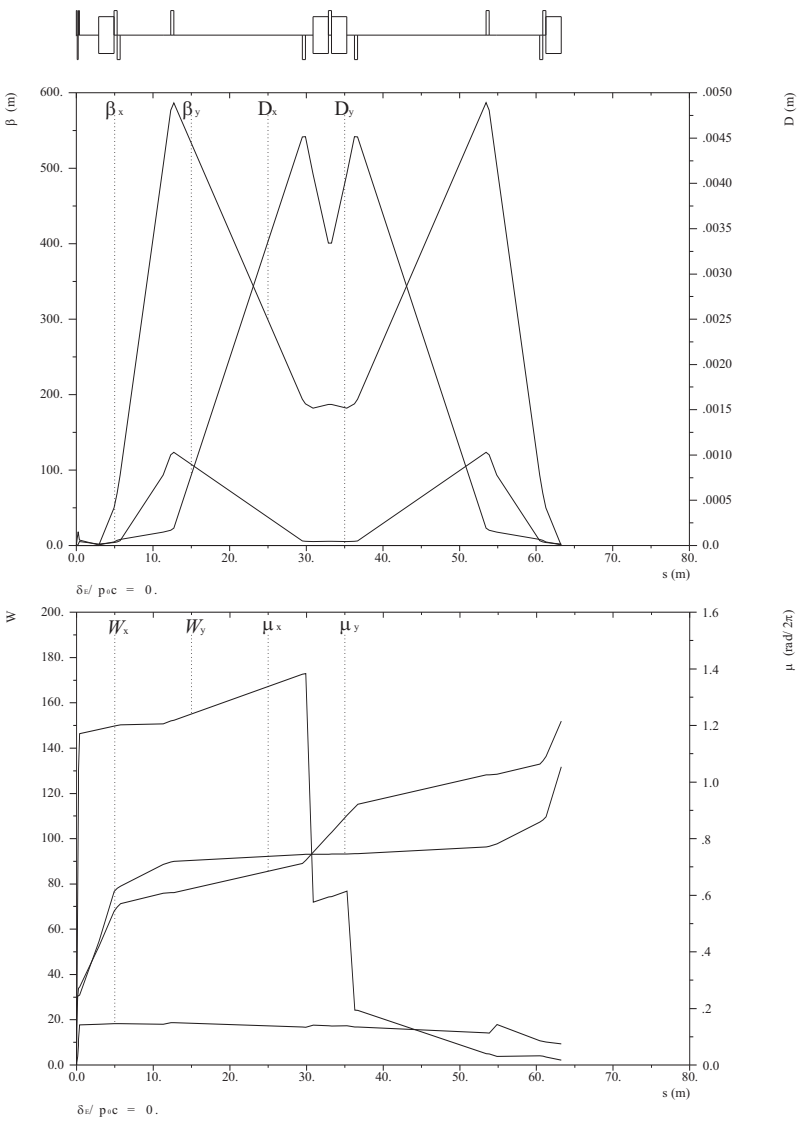

FIG. 11. The defocus nonlinear optics for the Laser-Compton cooling.

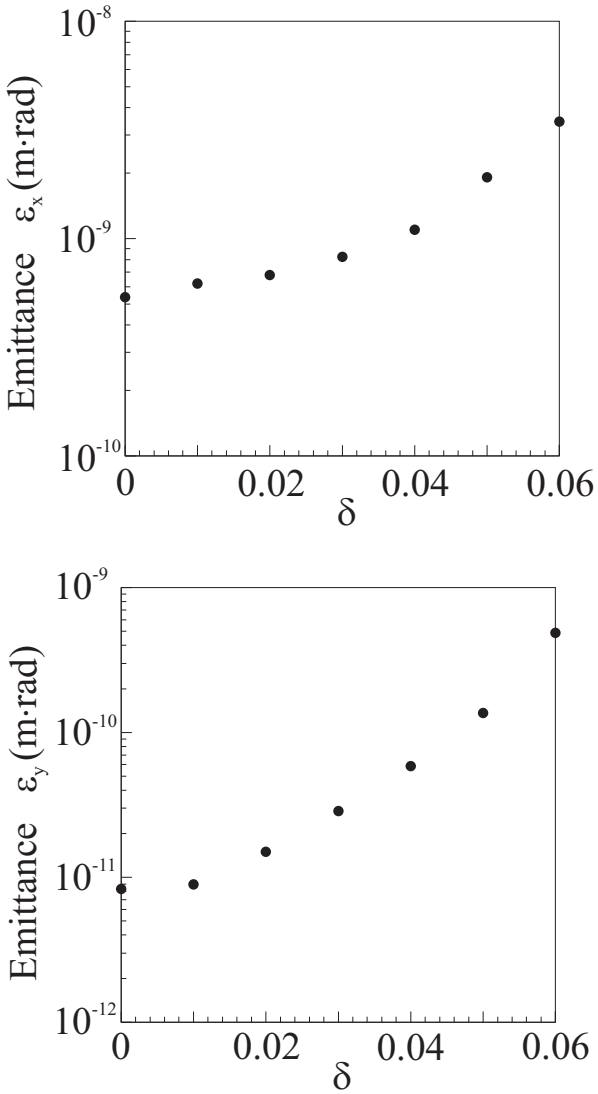

FIG. 12. Momentum dependence of the emittances in the defocus nonlinear optics.

ACKNOWLEDGMENTS

This work was supported in part by the U.S. Department of Energy under Contract No. DE-AC03-76SF00098.

---

[1] V. Telnov, Phys. Rev. Lett. **78**, 4757 (1997); *ibid.* **80**, 2747 (1998); V. Telnov in *Proceedings of the 15th Advanced ICFA Beam Dynamics Workshop on Quantum Aspects of Beam Physics*, Monterey, CA, 4-9 Jan 1998, BUDKERINP-98-33 (1998).

[2] P. Chen, T. Ohgaki, A. Spitkovsky, T. Takahashi, and K. Yokoya, Nucl. Instrum. and Methods Phys. Res. A **397**, 458 (1997).

[3] B.W. Montague and F. Ruggiero, CLIC-NOTE-37 (1987).

[4] K. Oide, Nucl. Instrum. Meth. Phys. Res. A **276**, 427 (1989); in *Proceedings of the DPF Summer Study on High Energy Physics in the 1990's*, Snowmass, CO, Jun 27-Jul 15 1988, SLAC-PUB-4806 (1988); in *Proceedings of the 1st Workshop on the Japan Linear Collider* (JLC), Tsukuba, Japan, Oct 24-25, 1989, KEK-Preprint-89-190 (1989).

[5] Zeroth-Order Design Report for the Next Linear Collider, LBNL-PUB-5424, SLAC-Report-474 (1996); JLC Design Study,

KEK-Report-97-1 (1997); Conceptual Design of a 500 GeV Electron Positron Linear Collider with Integrated X-Ray Laser Facility, DESY-97-048, ECFA-97-182 (1997).

[6] H. Grote and F.C. Iselin, The MAD Program (Methodical Accelerator Design) Version 8.19: User's Reference Manual, CERN-SL-90-13-AP (1996).

[7] P. Chen, K. Oide, A.M. Sessler, and S.S. Yu, Phys. Rev. Lett. **64**, 1231 (1990); in *Proceedings of the Fourteenth International Conference on High Energy Accelerators*, Tsukuba, Aug 22-26, 1989, SLAC-PUB-5060 (1989).